

Filling Control of the Mott Insulator Ca_2RuO_4

Hideto FUKAZAWA^{1,*} and Yoshiteru MAENO^{1,2}

¹*Department of Physics, Kyoto University, Kyoto 606-8502*

²*Core Research for Evolutional Science and Technology, Japan Science and Technology Corporation (CREST-JST), Kawaguchi 332-0012*

(Received October 25, 2018)

We have grown single crystals of electron doping system $\text{Ca}_{2-x}\text{La}_x\text{RuO}_4$ ($0.00 \leq x \leq 0.20$) by a floating zone method. The first order metal/non-metal transition and canted antiferromagnetic ordering occur for $0.00 < x < 0.15$, similar to those in the bandwidth controlled system $\text{Ca}_{2-x}\text{Sr}_x\text{RuO}_4$ (CSRO). However, comparing with CSRO, we found a rather different metallic ground state adjacent to the non-metallic ground state with canted antiferromagnetic order. Instead of short-range antiferromagnetic correlation found in CSRO ($0.20 \leq x < 0.50$), the metallic ground state of the present system is characterized by strong ferromagnetic correlation.

KEYWORDS: Ca_2RuO_4 , Mott insulator, metal-insulator transition, ruthenate, filling control, Sr_2RuO_4 Mott transition, floating zone method

§1. Introduction

The discovery of superconductivity in Sr_2RuO_4 ($T_c \simeq 1.5$ K) has attracted strong research interests because it is the first layered-perovskite superconductor without copper.¹⁾ In addition its spin-triplet superconductivity has promoted deeper investigation of its anisotropic and unconventional physical properties in both superconducting and normal states.^{2, 3, 4, 5, 6, 7)} The electronic properties of Sr_2RuO_4 reflecting strong electronic correlation imply that it is in the vicinity of Mott transition.¹⁾ In fact its isomorph Ca_2RuO_4 is a Mott insulator, which exhibits canted antiferromagnetic (CAF) ordering at 113 K (= T_N : Néel temperature) and insulator-”near” metal transition at 357 K (= T_{MI}) on heating.^{8, 9, 10, 11, 12)}

Recently it has been recognized that orbital degrees of freedom of t_{2g} states, originating from the low-spin $4d^4$ configuration of Ru^{4+} ions, play important roles in physical properties of quasi-two-dimensional Mott-transition system $\text{Ca}_{2-x}\text{Sr}_x\text{RuO}_4$ (CSRO).^{13, 14)} In CSRO, the metal-insulator (MI) or strictly speaking, metal/non-metal (M/NM) transition, occurs simultaneously with the first-order structural phase transition, which is attributable to the Jahn-Teller effect.^{14, 15)} Smaller ionic radius of Ca^{2+} ions ($r_{\text{Ca}} = 1.18$ Å) compared with that of Sr^{2+} ions ($r_{\text{Sr}} = 1.31$ Å) brings about the transition from quasi-tetragonal orthorhombic L-Pbca to orthorhombic S-Pbca structure below T_{MI} .¹⁶⁾ In the latter structure, it is expected that the bandwidth of t_{2g} orbitals becomes narrow and the band configuration changes to lower the electronic energy.^{13, 14, 15, 17)}

In CSRO, bandwidth is mainly controlled by substitution of Sr for Ca. The other essential procedure to modify the quasi-two-dimensional antiferromagnetic (AF) Mott insulator is filling control, by which high temperature superconductivity of cuprates appears. However, we should

take into account that ruthenates possess triply degenerate t_{2g} orbitals $4d_{xy}, 4d_{yz}, 4d_{zx}$; in contrast, cuprates possess only single orbital $3d_{x^2-y^2}$. Therefore, it is highly interesting to investigate how this multi-band structure of ruthenates would give rise to a different characteristic in M/NM transition by filling control.

It is natural to try substituting trivalent La for divalent Ca in order to alter the number of $4d$ electrons, since the ionic radius of La^{3+} ions ($r_{\text{La}} = 1.216$ Å) is between those of Ca^{2+} ions and Sr^{2+} ions. Accordingly, we grew single crystals of electron-doping system $\text{Ca}_{2-x}\text{La}_x\text{RuO}_4$ (CLRO) by a floating zone (FZ) method for the first time. It is vital to investigate these quasi-two-dimensional materials by using single crystals because of their strongly anisotropic physical properties.

In this paper we present the phase diagram of CLRO obtained from in-plane resistivity, specific heat and dc magnetization. CAF and non-metallic (NM) region exists just near the parent material Ca_2RuO_4 ($0.00 < x < 0.15$). The physical characteristics of this region is quite similar to those reported in CSRO ($0.00 < x < 0.20$).^{13, 14)} Metallic ground state appears with increasing x ($x \geq 0.15$). Nevertheless, the characteristics of the metallic region just above $x = 0.15$ is different from those of CSRO ($0.20 \leq x < 0.50$). It is rather similar to those of CSRO with $x \geq 0.50$. We discuss the origin of such electronic correlation in the metallic region.

Recently Cao *et al.* also studied this CLRO system, but by using single crystals prepared by a flux method using Cl-flux.¹⁸⁾ Physical properties of crystals prepared by a flux method often qualitatively differ from the intrinsic ones obtained by single crystals grown by a FZ method or by polycrystals prepared by a conventional solid-state reaction.^{8, 9, 10, 11, 12, 19)} Comparing with the results reported by Cao *et al.*, we clarify the intrinsic properties of CLRO.

* E-mail address: hideto@scphys.kyoto-u.ac.jp

§2. Experimental

We have recently succeeded in growing single crystals of $\text{Ca}_{2-x}\text{La}_x\text{RuO}_4$ ($0.00 \leq x \leq 0.20$) by a FZ technique with an infrared image furnace.²⁰⁾ Typical condition of the single crystal growth has already been described.¹²⁾

We estimated the concentration of La in as-grown crystals of CLRO by energy dispersive x-ray (EDX) analysis: $x = 0.00(1)$, $0.02(1)$, $0.06(2)$, $0.11(2)$, $0.18(2)$ and $0.18(2)$ corresponding to the nominal concentration of $x = 0.00$, 0.015 , 0.05 , 0.10 , 0.15 and 0.20 in the polycrystalline feed rods used for single crystal growth. Although the results by EDX analysis for the nominal concentrations of $x = 0.15$ and 0.20 coincide with each other, we designate x as the concentration in the polycrystalline feed rods since the other physical properties of the single crystals did systematically change with the increase of nominal concentration.

Braden *et al.* reported that after annealing treatment in oxygen, polycrystalline $\text{Ca}_2\text{RuO}_{4+\delta}$ with $\delta = 0.07(1)$ exhibits MI transition at about 150 K.¹⁰⁾ In order to investigate the intrinsic properties of CLRO, we determined the amount of oxygen δ in $\text{Ca}_{2-x}\text{La}_x\text{RuO}_{4+\delta}$ by thermogravimetric analysis (TGA). We found that δ for $x = 0.00$ and 0.20 were $0.00(1)$ and $0.01(1)$, respectively. These results ensure that all the as-grown crystals of CLRO are stoichiometric within experimental accuracy. Therefore, we may safely assume that the number of $4d$ electrons in the t_{2g} orbitals increases with x . In this paper, we will refer to stoichiometric Ca_2RuO_4 as S-CRO and oxidized Ca_2RuO_4 ($\text{Ca}_2\text{RuO}_{4+\delta}$) as O-CRO.

We examined the structure of the as-grown samples at room temperature by x-ray diffraction of powdered single crystals. For $x = 0.00$ and 0.015 , the x-ray patterns agreed with that of orthorhombic structure. For the other x , the x-ray pattern fit well to tetragonal structure. In Fig. 1 we summarize the lattice parameters of CLRO and CSRO.¹⁴⁾ Here, we divide a and b of the orthorhombic samples by $\sqrt{2}$ for the sake of convenience. As we will describe below, orthorhombic samples exhibit non-metallic behavior; however, tetragonal samples exhibit metallic behavior. In tetragonal phase, a ($= b$) is longer than that for CSRO with corresponding x , while c is shorter. With increasing x , a increases slightly while c remains nearly unchanged.

We measured the in-plane resistivity by a standard four-probe method below 355 K and the specific heat by a relaxation method between 1.8 and 300 K. We investigated the dc magnetization with a commercial SQUID magnetometer between 1.8 and 700 K.²¹⁾

§3. Results

3.1 Phase diagram

First, we summarize the physical properties of CLRO ($0.00 \leq x \leq 0.20$) in the phase diagram in Fig. 2. In this phase diagram, we denote the transition temperatures observed on heating. Instead of M/NM transition temperature for $x = 0.015$, we plot the first-order phase transition temperature of the magnetization, since we did not extend the resistivity measurement to high enough temperature. Indeed the first-order phase transition temper-

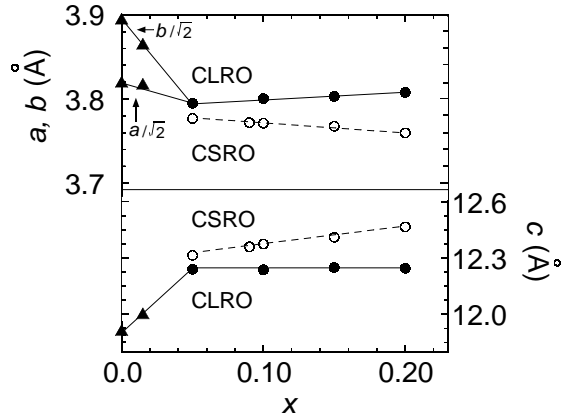


Fig. 1. Lattice parameters of $\text{Ca}_{2-x}\text{La}_x\text{RuO}_4$ (solid triangles: $x = 0.00$ and 0.015 , solid circles: $0.05 \leq x \leq 0.20$) at room temperature. We have divided the in-plane parameters of the orthorhombic samples by $\sqrt{2}$. The lattice parameters of $\text{Ca}_{2-x}\text{Sr}_x\text{RuO}_4$ (open circles) are also shown for comparison.¹⁴⁾ The change from orthorhombic structure (triangles) to tetragonal structure (circles) coincides with that of the transport properties from non-metallic behavior to metallic one with x .

ature of the magnetization coincides with MI or M/NM transition temperature for $x = 0.00$, 0.05 and 0.10 .

In the non-metallic region, CAF ordering occurs below T_N . This temperature is clearly less than the M/NM transition temperature $T_{M/NM}$. $T_{M/NM}$ approaches T_N with increasing x and both vanish below $x = 0.15$. We draw the expected phase boundary with a broken line in Fig. 2. In the metallic region, apparent Curie-Weiss law is realized.

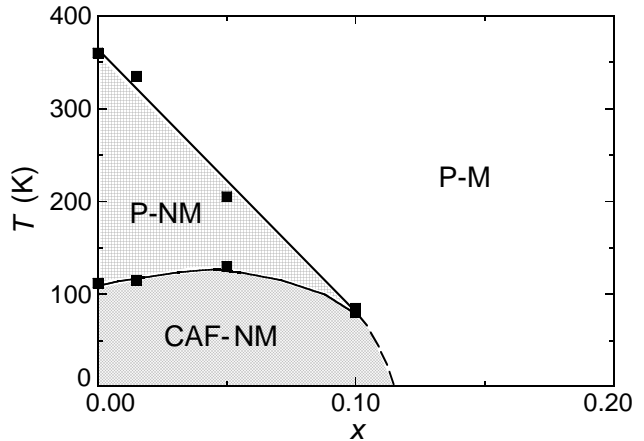


Fig. 2. Phase diagram of $\text{Ca}_{2-x}\text{La}_x\text{RuO}_4$. P: paramagnetic, CAF: canted antiferromagnetic, -M: metal, and -NM: non-metal. The M/NM transition is associated with the first-order structural transition.

In this chapter, we describe the in-plane resistivity, specific heat and dc magnetization, which serve the basis for the phase diagram.

3.2 In-plane resistivity

In Fig. 3, we show the in-plane resistivity $\rho_{ab}(T)$ of CLRO below 355 K. The data plotted were obtained on cooling below room temperature and on heating above room temperature in helium atmosphere. We measured the dc resistivity down to 4.2 K for all the samples and the ac resistivity down to 0.5 K for $x = 0.15$ and down to 50 mK for $x = 0.20$.

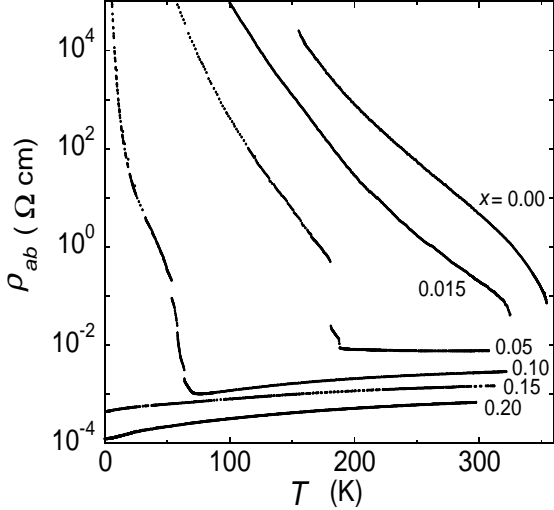


Fig. 3. The in-plane resistivity $\rho_{ab}(T)$ of CLRO ($0.00 \leq x \leq 0.20$) below 355 K. The metal/non-metal transition temperature decreases with x . Metallic ground state appears at $x = 0.15$.

Above 355 K, the measurement had to be terminated for S-CRO since the samples shattered at this temperature, owing to the first-order structural phase transition. This transition nearly coincides with the insulator-”near” metal transition temperature of the Ca_2RuO_4 crystals prepared by a flux-method.¹¹ The resistivity exhibits insulating behavior on cooling down to about 150 K. Below 150 K, the ρ_{ab} became too large for our present measurement setup. Nevertheless we confirmed that below this temperature the resistivity remains higher than the value at 150 K.

For $x = 0.015$, the crystals did not shatter at least up to 325 K. For $x = 0.05$ and 0.10, the $\rho_{ab}(T)$ exhibits metallic behavior on cooling but suddenly increases by two orders of magnitude at 188 K ($x = 0.05$) and at 77 K ($x = 0.10$). Below each characteristic temperature, the ρ_{ab} becomes non-metallic and monotonously increases beyond $10^5 \Omega\text{cm}$ on cooling. On warming, the crystals again exhibit the hysteretic M/NM transition at 206 K ($x = 0.05$) and at 84 K ($x = 0.10$). Hence, the M/NM transition in CLRO is most probably of the first order. The resistivity on warming above $T_{M/NM}$ does not recover the same value that was obtained on cooling. This is clearly due to micro cracks, actually found after the measurement, which are most likely introduced by the first-order structural phase transition. From this result we deduce that the M/NM transition coincides with the first-order structural phase transition in CLRO, as reported in the parent material S-CRO and CSRO.^{11,13,15} Cao *et al.* also reported the same phe-

nomenon.¹⁸ However, we notice that the resistivity at low temperatures show no saturation behavior, in contrast with the report by Cao *et al.*¹⁸

For $x = 0.15$ and 0.20, the $\rho_{ab}(T)$ almost linearly decreases on cooling down to 1.0 K ($x = 0.15$) and 0.5 K ($x = 0.20$). The resistivity saturates below 1.0 K ($x = 0.15$) and 0.5 K ($x = 0.20$) with the residual resistivities of $\rho_0 = 4.5 \times 10^2 \mu\Omega\text{cm}$ ($x = 0.15$) and $\rho_0 = 1.3 \times 10^2 \mu\Omega\text{cm}$ ($x = 0.20$). We do not find any sign of superconductivity at least down to 0.5 K ($x = 0.15$) and 50 mK ($x = 0.20$) so far.

3.3 Specific heat

In Fig. 4, we plot the specific heat divided by temperature, C_P/T , for $x = 0.00, 0.15$ and 0.20 against T^2 below 25 K. We could not measure the specific heat of the crystals for $x = 0.05$ and 0.10 since the crystals attached to the sapphire plate with vacuum grease always came off on cooling through $T_{M/NM}$.

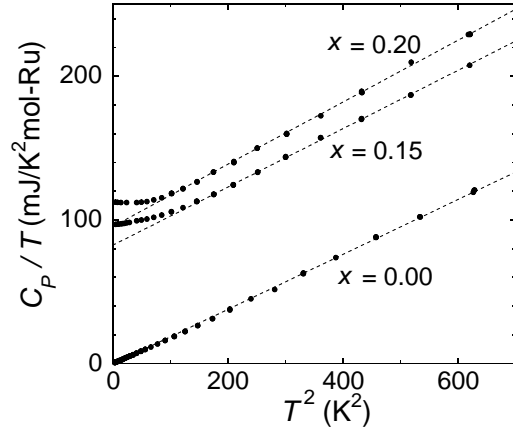


Fig. 4. Electronic specific heat C_P/T vs T^2 of $\text{Ca}_{2-x}\text{La}_x\text{RuO}_4$.

We performed fitting the data to the following formula below 25 K for $x = 0.00$ and between 10 and 25 K for $x = 0.15$ and 0.20:

$$C_P/T = \gamma + \beta T^2. \quad (3.1)$$

Electronic specific heat coefficient γ directly reflects the density of states (DOS) at the Fermi level, $D(\epsilon_F)$. From β , we can deduce the Debye temperature by $\Theta_D = (12\pi^4 N k_B / 5\beta)^{1/3}$, where $N (= 7N_A)$: N_A is the Avogadro number) is the number of atoms per mole and k_B is the Boltzmann constant. We summarize the parameters (γ , Θ_D) obtained from the data in Table I.

The result that γ is equal to $0.0 \pm 0.2 \text{ mJ/K}^2\text{mol-Ru}$ for S-CRO indicates an energy gap at the Fermi level in the ground state. Hence, S-CRO is an insulator.

γ for the metallic samples is by a factor of more than two larger than that of the spin-triplet superconductor Sr_2RuO_4 , $37.5 \text{ mJ/K}^2\text{mol-Ru}$.^{6,5} Slight deviation from eq. (3.1) below 10 K might reflect strong magnetic fluctuation. All the values of Θ_D , including that of Sr_2RuO_4 ($\Theta_D = 410 \pm 10\text{K}$), are almost the same.²²

Table I. Electronic specific heat coefficient γ and Debye temperature θ_D of $\text{Ca}_{2-x}\text{La}_x\text{RuO}_4$.

x	γ (mJ/K ² mol-Ru)	θ_D (K)
0.00	0.0(2)	400
0.15	82(1)	420
0.20	95(1)	420

3.4 Magnetization

3.4.1 Magnetization of S-CRO

In Fig. 5, the anisotropic dc magnetic susceptibilities, $M(T)/H \equiv \chi(T)$ ($\mu_0 H = 1$ T), in zero-field-cooled (ZFC) sequence are shown for S-CRO. Below 320 K, we used a uniaxial sample rotator. The directions of the applied field were along the [100], [010] and [001] axes of the orthorhombic structure with Pbc_a symmetry. By adjusting the [001] axis to be parallel to the rotational axis, we applied the magnetic field parallel to the [100] axis and the [010] axis. Between 320 and 700 K, we measured the $\chi(T)$ along the [001] axis and along one of the axes in the ab plane on heating and on cooling.

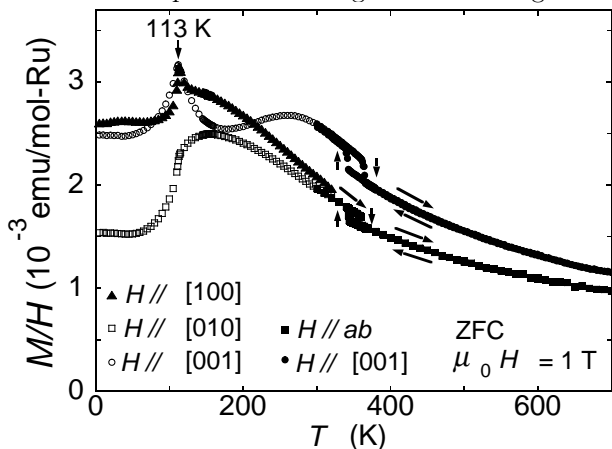


Fig. 5. The magnetic susceptibilities $\chi(T)$ of stoichiometric Ca_2RuO_4 (S-CRO). S-CRO exhibits CAF ordering below 113 K. The hysteretic behavior around 350 K corresponds to metal-insulator transition, which coincides with the first-order structural phase transition.¹¹⁾

We found slight hysteresis between the data of ZFC sequence and field-cooled (FC) sequence below about 160 K. However, the magnitude of this hysteresis is negligible compared with that of O-CRO as we show in Fig. 6. Therefore, let us concentrate on the ZFC data of S-CRO.

The prominent features in Fig. 5 are sharp cusps of χ along the [100] and [001] axes at 113 K. Below this temperature, χ along each of the three axes decreases rapidly on cooling. This is ascribable to CAF ordering below $T_N = 113$ K.¹²⁾

Between T_N and 320 K, χ along each axis cannot be fitted to the Curie-Weiss law:

$$\chi(T) = \chi_p + \frac{C}{T - \theta_{CW}}, \quad (3.2)$$

Here, χ_p represents the paramagnetic component (*eg.*

Pauli paramagnetism and van Vleck orbital paramagnetism, as well as diamagnetic susceptibility of the ion cores). C is the Curie constant and θ_{CW} is the Curie-Weiss temperature. It is surprising that $\chi_{[001]}(T)$ has a broad peak at around 260 K since no static magnetic ordering was found by neutron diffraction.¹⁰⁾ This temperature is substantially higher than T_N ; we cannot attribute this to the influence of CAF correlation.

On heating χ_{ab} and χ_c abruptly decrease at 360 K corresponding to T_{MI} . On cooling χ_{ab} and χ_c recover the value in the insulating region at 344 K. This hysteretic behavior of the magnetization indicates the phase transition of the first order. χ_{ab} and χ_c apparently follow the Curie-Weiss law between 360 and 700 K, $\theta_{CW} = -78$ K parallel to the ab plane and -73 K parallel to the c axis. The total spin S derived by $C = N_A g^2 S(S+1) \mu_B^2 / 3k_B$ (μ_B : the Bohr magneton) is equal to 0.8 parallel to the ab plane and 0.9 parallel to the c axis, reflecting the nearly localized moment $S \simeq 1$. The other parameter χ_p is consistent with that obtained from polycrystalline samples and its magnitude is negligible.¹⁴⁾

3.4.2 Magnetization in the non-metallic region

In Fig. 6, we plot the magnetic susceptibility along the [100] axis for S-CRO and CLRO ($x = 0.015$). We add the in-plane magnetic susceptibility of single crystals of O-CRO, which was prepared by annealing the single crystals of S-CRO under 12.0 MPa of oxygen at 540 °C for 90 hours. The single crystals of O-CRO exhibited M/NM transition at 290 K on cooling but shattered at 320 K on heating (not shown). We could not determine the amount of oxygen δ in $\text{Ca}_2\text{RuO}_{4+\delta}$ by TGA, since the mass of single-phase crystals was not large enough for high-precision TGA. Thus, we estimated $\delta \sim 0.04$ from the difference of the mass before and after annealing. This estimation is consistent with the result that $T_{M/NM}$ of single-crystalline O-CRO, ~ 320 K, is between that of S-CRO with $\delta = 0.00(1)$, ~ 350 K, and that of polycrystalline O-CRO with $\delta = 0.07(1)$, ~ 150 K.¹⁰⁾ We may regard O-CRO as another filling control system derived from S-CRO: a hole-doping system.

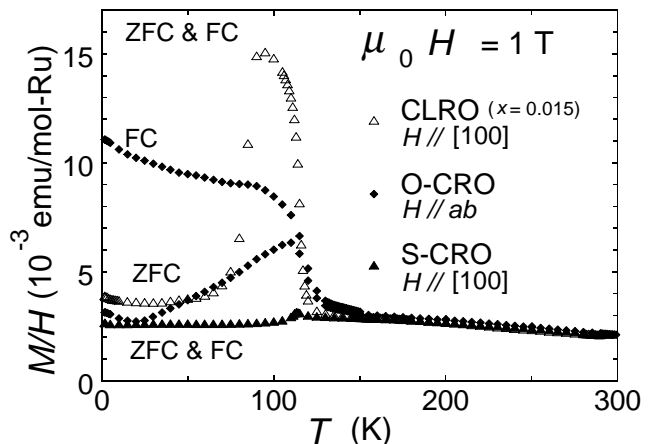


Fig. 6. The $\chi_{[100]}(T)$ of S-CRO and CLRO ($x = 0.015$) and the $\chi_{ab}(T)$ of oxidized Ca_2RuO_4 . Slight carrier-doping induces ferromagnetic component in the magnetically ordered region.

From the large magnetization and its hysteresis shown in Fig. 6, we may conclude that ferromagnetic (FM) component appears in the AF ground state of S-CRO once carriers are introduced into the t_{2g} orbitals. Despite the prominent peak along the [100] axis of CLRO ($x = 0.015$), $\chi(T)$ along either the [010] axis or the [001] axis does not show any corresponding peak (not shown). Instead the $\chi_{[010]}$ and the $\chi_{[001]}$ of CLRO ($x = 0.015$) are similar to those of S-CRO in magnitude. Static AF ordering is observed by neutron diffraction in S-CRO and in polycrystalline O-CRO with $\delta = 0.07(1)$ below 150 K in spite of the presence of finite FM component.¹⁰ This result supports that the magnetic ordering of single-crystalline O-CRO below 160 K is also ascribable to AF ordering with FM component.

For CLRO ($x = 0.015$), we found the hysteretic change of χ at 334 K on heating and at 323 K on cooling (not shown). This behavior is essentially the same as that seen in S-CRO at around 350 K. The crystals after the measurement had shattered. We infer that this first-order phase transition comes from the structural phase transition, which coincides with M/NM transition.

In Fig. 7, we plot the magnetic susceptibilities $\chi_{[100]}(T)$ for $x = 0.00$ and 0.015 and the $\chi_{ab}(T)$ for $0.05 \leq x \leq 0.20$ in ZFC and FC sequences. Only the data for $x = 0.05$ and 0.10 show the strongly hysteretic behavior below 170 K ($x = 0.05$) and 75 K ($x = 0.10$).

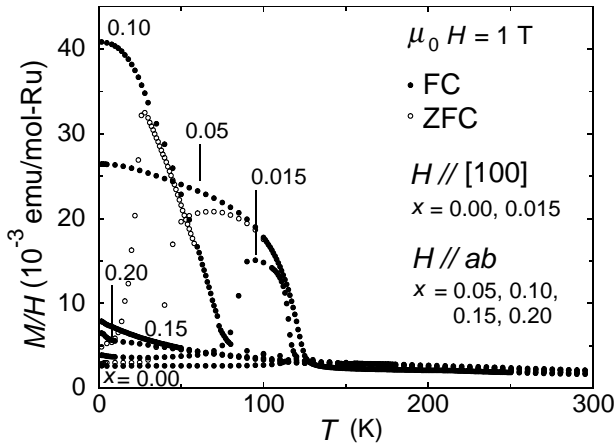


Fig. 7. The $\chi_{[100]}(T)$ for $x = 0.00$ and 0.015 and the $\chi_{ab}(T)$ for $0.05 \leq x \leq 0.20$. In the non-metallic region, canted anti-ferromagnetic ordering occurs below T_N . Apparent Curie-Weiss behavior was found for $x = 0.15$ and 0.20 down to 1.8 K.

As also reported by Cao *et al.*, the FM component emerges gradually with x .¹⁸ We attribute this to the alteration of the interlayer magnetic mode of CAF ordering as we will discuss in §4. 2. 3.

3.4.3 Magnetization in the metallic region

In the metallic region, there is no sign of magnetic ordering. Instead, apparent Curie-Weiss law is realized down to low temperatures. In this subsection, we describe the magnetization of CLRO for $x = 0.15$ and 0.20.

We fit the data to eq. (3.2) above 100 K. We obtain the negative Curie-Weiss temperature and finite paramagnetic component $\chi_P (= 5\text{-}6 \times 10^{-4}$ emu/mol-Ru). Since we consider the conducting electrons all originating from

the same t_{2g} orbitals, it is not natural to expect the two magnetic species: the nearly localized moment giving the Curie-Weiss term and the itinerant electrons giving the paramagnetic component χ_P in eq. (3.2). (An alternative interpretation is recently given by Anisimov *et al.*¹⁷)

In the presence of strong correlation and spin fluctuation among itinerant electrons, it is expected that the Pauli susceptibility is modified to $\chi_P(T)$ given by²³

$$\chi_P(T) = \frac{\chi_0(T)}{1 - \alpha\chi_0(T) + \lambda(T)}, \quad (3.3)$$

$$\chi_0(T) = \chi_0(1 + c_0 T^2).$$

Here, α is the correlation energy, χ_0 is the Pauli susceptibility of non-interacting system, c_0 is the coefficient depending on DOS at around the Fermi level and is ordinarily proportional to T_F^{-2} , $\lambda(T)$ is proportional to T in the presence of FM fluctuation. Although $\chi_P^{-1}(T)$ is approximately proportional to $a_0 T + b_0$ ($a_0, b_0 > 0$) which gives apparent negative Curie-Weiss temperature, it exhibits the slight curvature of $d^2(\chi_P^{-1})/dT^2 > 0$ or < 0 , since $\chi_0(T)$ contains the $c_0 T^2$ term. In fact, $\chi_{ab}^{-1}(T)$ for $x = 0.15$ and 0.20 gives the negative Curie-Weiss temperature and exhibits such temperature dependence above 1.8 K. Consequently, the experimental $\chi_{ab}(T)$ for $x = 0.15$ and 0.20 is well ascribed as the Pauli susceptibility in the presence of FM fluctuation.

Although it is not a simple Fermi liquid, it is worthwhile to evaluate the Wilson ratio R_W in order to assess the magnetic correlation among the itinerant electrons. R_W is given by the following formula:

$$\begin{aligned} R_W &= \frac{\chi_P(0 \text{ K}) / \chi_0}{\gamma / \gamma_0} \\ &= \frac{4\pi^2 k_B^2 \chi_P(0 \text{ K})}{3(g\mu_B)^2 \gamma}. \end{aligned} \quad (3.4)$$

Here, $\chi_P(0 \text{ K})$ is the experimental Pauli susceptibility in the limit of 0 K, γ is the electronic specific heat coefficient obtained from experiment, and γ_0 is that of non-interacting system.

To evaluate R_W , we use the experimental value $\chi_{ab}(2 \text{ K})$ to approximate $\chi(0 \text{ K})$, the electronic specific heat coefficient γ in table I. Wilson ratio R_W are 6.9 for $x = 0.15$ and 4.8 for $x = 0.20$. R_W for both samples is considerably larger than the value one or two, which are expected for a non-interacting electron system or for a strongly correlated electron system, respectively. This result is in accord with the existence of additional FM fluctuation among the itinerant electrons over the mass enhancement at least for $x = 0.15$ and 0.20. These magnetic characteristics in the metallic region of CLRO are similar to those reported in CSRO for $x \geq 0.50$.^{13, 14}

§4. Discussion

4.1 Mott insulator Ca_2RuO_4

In our previous papers we have revealed that S-CRO is a Mott insulator on the basis of the results with single crystals grown by a FZ method and polycrystalline samples made by a conventional solid state reaction.^{8, 10, 12} However, Cao *et al.* had implied that Ca_2RuO_4 is a lo-

calized metal from the results of the flux-grown crystals, since γ is about 4 mJ/K²mol-Ru and resistivity exhibits a variable-range-hopping (VRH) behavior.⁹⁾ In addition Mazin and Singh also agreed with this conclusion for the reason that a small Fermi surface exists in S-CRO in their local density approximation calculation.²⁴⁾ Although γ is still finite, Cao and Alexander *et al.* have recently agreed with our previous claim and stated that Ca₂RuO₄ is not a localized metal but a Mott insulator.^{11,18)} Mazin and Singh have also agreed with the fact,²⁵⁾ since the intrinsic γ of S-CRO is 0.0(2) mJ/K²mol-Ru, which is obtained from high quality single crystals grown by a FZ method.¹²⁾ We note that experimental finite γ is attributable to the off stoichiometry of the single crystals, since Ca₂RuO₄ is quite sensitive to annealing treatment.

S-CRO exhibits CAF ordering below 113 K. The associated spin canting is ascribable to the Dzyaloshinsky-Moriya (DM) interaction.^{8,12)} This suggests that spin-orbit coupling is important in S-CRO. According to the spin-resolved circularly-polarized photoemission and O 1s x-ray absorption spectroscopy (XAS) on our single crystals of S-CRO performed by Mizokawa *et al.*, the spin-orbit coupling indeed plays an important role in S-CRO.²⁶⁾ Here, let us discuss the origin of the broad peak of $\chi_{[001]}(T)$ of S-CRO at around 260 K (Fig. 4). Mizokawa *et al.* showed that the orbital angular moment exists along the [001] axis at 300 K, but on cooling to 90 K, it alters its direction to within the *ab* plane. In addition, they showed, by calculation, that the form of the RuO₆ octahedra in S-CRO dictates the direction of the orbital moment; orbital moment is along the [001] axis for elongated and regular RuO₆ octahedra, while perpendicular to the [001] axis for flattened RuO₆ octahedron. Neutron diffraction on polycrystalline S-CRO has revealed that the RuO₆ octahedra is elongated above 300 K, regular at around 300 K and flattened below 300 K.^{10,15)} We expect the magnetic anisotropy to be influenced by changes in the direction of the orbital moment, as well as by the associated polarization of the spin moment. The experimental result that $\overline{\chi_{ab}}$ ($\equiv (\chi_{[100]} + \chi_{[010]})/2$) is smaller than $\chi_{[001]}$ above 200 K but becomes larger than $\chi_{[001]}$ between 150 and 200 K (Fig. 5) supports this interpretation.²⁸⁾

4.2 Non-metallic region

4.2.1 Origin of non-metallic ground state

In the parent material S-CRO, the metal to insulator transition coincides with the first-order structural phase transition of the quasi-tetragonal L-Pbca phase to the orthorhombic S-Pbca phase as we noted in §1.^{11,15)} In CSRO and the hole-doping system O-CRO, it is revealed by neutron diffraction on polycrystalline samples that the situation is almost the same.^{10,14,15)} In CLRO investigated here, non-metallic crystals have the orthorhombic structure whereas metallic crystals have the tetragonal structure at room temperature. Furthermore, M/NM transition in this system is also of the first order. These results indicate that the metal to non-metal transition coincides with the first-order structural phase transition between the high-temperature L-Pbca phase to the low-

temperature phase in CLRO. Neutron diffraction experiment is necessary to confirm that the low-temperature structure is indeed S-Pbca even for $x \neq 0.00$.

The change from the L-Pbca phase to the S-Pbca phase is characterized by the flattening of the RuO₆ octahedra. The lattice parameters *a* and *b* are elongated and *c* is shrunk reflecting the flattening. The flattening of the RuO₆ octahedra is expected to greatly influence the crystal field which mainly determines the electron occupancy in the triply degenerate orbital state of ruthenate. By the flattening, nearly degenerate *t_{2g}* orbitals is expected to form the lowest *4d_{xy}* orbital and the lower and the upper Hubbard band which originates from the nearly doubly degenerate *4d_{yz}* and *4d_{zx}* orbitals. O 1s XAS on S-CRO has clarified that the *4d_{xy}* orbital is energetically lower than the other *4d_{yz}* and *4d_{zx}* orbitals at 90 K, supporting our expectation.²⁶⁾ Such structural change is attributable to the Jahn-Teller effect.²⁷⁾

The physical properties in the non-metallic region of CLRO is qualitatively quite similar to those of the Mott insulator S-CRO. Hence, we infer that the ground state of CLRO in the non-metallic region is in a broad sense an Mott insulator. However, this non-metallic phase is more appropriately described by the Anderson localization of the excess *4d* electrons introduced by La substitution.

We did not find the saturation behavior of the resistivity at low temperatures in the non-metallic region for any *x*, in contrast with the observation in the flux-grown crystals ($0.07 \leq x \leq 0.11$: $T_{M/NM} \leq 210$ K).¹⁸⁾ Such behavior suggests that delocalized electrons exist in the flux-grown crystals. Nevertheless, magnetic properties of single crystals grown both by a FZ method and by a flux method are almost the same.

4.2.2 Conduction mechanism

For ordinary semiconducting materials with band gaps, the following formula is often used:²⁹⁾

$$\rho_{ab}(T) = A_0 \exp\left(\frac{\Delta_n}{T}\right)^{\frac{1}{n+1}} \quad (n = 0, 1, 2, 3). \quad (4.1)$$

For $n = 0$, the formula represents the activation-type conductivity: Δ_0 is the activation energy. For the other n , eq. (4.1) represents the n dimensional VRH without interaction among the localized electrons: Δ_n is the characteristic temperature. If we consider the Coulomb interaction between localized electrons, n is unity for three dimensional system.³⁰⁾ In the VRH mechanism, we should notice that DOS at the Fermi level, $D(\varepsilon_F)$, is finite.

Each ρ_{ab} -curve for $0.00 \leq x \leq 0.10$ has an inflection point below $T_{M/NM}$ (Fig. 3). We fit the data of ρ_{ab} below the inflection point and found at least $n \neq 0$ for all the samples and $n = 1$ for $x = 0.10$. Fitting with $n = 1, 2$ or 3 gave equally satisfactory results for $x = 0.00, 0.015$ and 0.05. Cao *et al.* reported that they found n equal to 1 for the samples of CLRO which did not exhibit saturation behavior of the resistivity.¹⁸⁾

In CLRO, La substitution would bring a random potential, which could localize the itinerant electrons. In fact, $n \neq 0$ indicates that conduction mechanism is not the simple activation-type but VRH. At the same time, we expect strong electronic correlation since the parent

material S-CRO is the Mott insulator. Thus, $n = 1$ for $x = 0.10$ suggests that the so-called soft Coulomb gap exists at the Fermi level. Consequently, we conclude that conduction mechanism in the non-metallic region is VRH with a small gap formed by strong electronic correlation.

Finally we note that the activation energy between 150 and 250 K is about 0.2 eV for S-CRO which is consistent with the previous results.^{8,9,11,31)} This activation energy diminishes with increasing x .

4.2.3 Magnetic correlation

Neutron diffraction on polycrystalline S-CRO and O-CRO samples revealed that there are two kinds of magnetic modes for static AF ordering in S-CRO and O-CRO: A-centered and B-centered. S-CRO has two coexisting modes: A-centered (major phase) and B-centered (minor phase). This is in contrast with O-CRO, which has only one mode: B-centered. A very small magnetic hysteresis in S-CRO indicates that it contains B-centered domains as a minor phase.

In order to explain AF ordering in S-CRO and O-CRO, CAF order has been proposed.^{8,10,12)} By taking account of DM interaction associated with spin-orbit coupling, we modify the spin arrangements, which are depicted in ref. 10, consistent with the rotation and tilt configuration of RuO_6 octahedra in Pbca symmetry and with magnetization (Fig. 8). Nearly the same arrangements have also been discussed by Braden *et al.*¹⁰⁾ However, we propose to include the component of the canted moments along the $[001]$ axis, which is necessary to explain the sharp peak in $\chi_{[001]}(T)$ of S-CRO at 113 K (Fig. 5)¹²⁾: solid circles in open circles denote that the $[001]$ component of canted moments is positive, while crosses in open circles denote negative. The spin canting will induce finite moment (big arrow) only along the $[100]$ axis within a RuO_2 plane. These canted moments cancel out between neighboring RuO_2 planes in the A-centered arrangement; they add up to finite FM component along the $[100]$ axis in the B-centered one. Consequently, three-dimensional AF ordering occurs in the A-centered mode, whereas FM component appears along the $[100]$ axis in the B-centered AF ordering. We attribute magnetic structures in S-CRO and O-CRO to these kinds of CAF ordering originating from the two magnetic modes and the spin canting.

We found a peak in $\chi(T)$ of CLRO for $x = 0.015$ only along the $[100]$ axis at around 95 K (Fig. 6) and no hysteric behavior between ZFC and FC sequences. This remarkable temperature dependence is explained if the B-centered mode is more stable just below T_N , though the A-centered mode is dominant in the ground state. In contrast, $\chi_{ab}(T)$ of CLRO for $x = 0.05$ and 0.10 in both ZFC and FC sequences is qualitatively quite similar to that of O-CRO. From these results, magnetically ordered phase of CLRO may also be ascribable to CAF ordered one, in which the B-centered mode becomes more stable than the A-centered one with increasing x or T . This interpretation is in sharp contrast with that by Cao *et al.*, since they claimed that the FM component in the non-metallic region is due to the Stoner enhancement originating from the itinerant electrons introduced by La

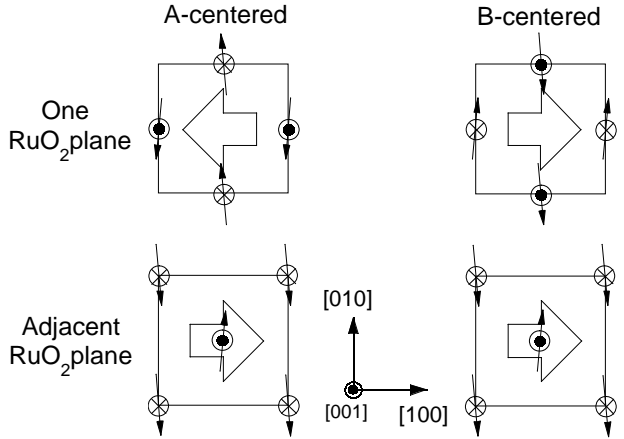


Fig. 8. Schematic spin configuration of CAF ordering in S-CRO and O-CRO consistent with neutron diffraction and magnetization.^{8,10,12)} Solid circles in open circles denote that the $[001]$ component of canted moments is positive, while crosses in open circles denote negative. In A-centered mode, finite moments induced by spin canting (big arrow) cancel out between neighboring RuO_2 planes. In B-centered mode, however, finite moments induce FM component along the $[100]$ axis.

substitution.¹⁸⁾

4.3 Metallic region

The ground state of CLRO for $x = 0.15$ and 0.20 is metallic. Considerably large γ suggests that finite DOS appears by La substitution and that strong electronic correlation exists in the metallic state. In this subsection, we discuss the physical properties of CLRO for $x \geq 0.15$.

The resistivity exhibits nearly linear temperature dependence. Hence, we may conclude that the ground state is at least not a simple Fermi liquid. In this region, we did not find any evidence for short-range AF correlation, which is the main characteristic of the metallic state adjacent to the M/NM boundary in CSRO ($0.20 \leq x < 0.50$).^{13,14)} Instead, the magnetic properties of CLRO in this region is similar to those in CSRO with $x \geq 0.50$. Considerably large Wilson ratio for $x = 0.15$ and 0.20 indicates that FM fluctuation is strong in this region. The origin of FM correlation may be associated with the van-Hove singularity and the resulting Stoner enhancement,^{32,24,33)} which itinerant electron system in quasi-two-dimensional ruthenates generally exhibit.

4.4 Filling control of Ca_2RuO_4

The ground state of CLRO ($0.00 < x < 0.15$) is CAF-NM. Almost the same CAF-NM ground state is realized in CSRO ($0.00 < x < 0.20$).^{13,14)} The important coincidence between the both systems is that M/NM transition occurs simultaneously with the first-order structural phase transition and that CAF ordering occurs at some temperature which is lower than T_N . We concluded that both ground states are in a broad sense Mott insulators.^{13,14)} These non-metallic ground states are unstable because slight La or Sr substitution for Ca will induce metallic ground states. Concerning CSRO, only bandwidth of nearly triply degenerate t_{2g} orbitals is controlled

by substituting divalent Sr for equivalent Ca. In CLRO, the bandwidth is also influenced by substituting trivalent La for heterovalent Ca. However, the experimental fact that metallic ground state in CLRO appears somewhat above 0.10 less than the corresponding boundary in CSRO at $x = 0.20$ indicates that filling control (electron-doping) in the t_{2g} orbitals is effective in destroying the non-metallic ground state, since the smaller La^{3+} ions cannot more effectively change the bandwidth than the larger Sr^{2+} ions. Cao *et al.* also noted this from independent results.¹⁸⁾ The metallic ground state of CLRO with $x \geq 0.15$ is rather different from that of CSRO with $0.20 \leq x < 0.50$ but is similar to that of CSRO with $x \geq 0.50$. This result also implies that the filling control changes the parent compound more rapidly.

Unlike cuprates, the first-order M/NM transition occurs simultaneously with the structural phase transition in CLRO, indicating the importance of Jahn-Teller effect. This effective filling control through the *orbital degeneracy tuning* brings a metallic phase with FM fluctuation in CLRO. This is quite in contrast with the filling control of half-filled single orbital, which brings a metallic (or superconducting) phase with AF fluctuation in cuprates.

§5. Conclusion

We have succeeded in growing single crystals of electron doping system $\text{Ca}_{2-x}\text{La}_x\text{RuO}_4$ ($0.00 \leq x \leq 0.20$) by a FZ method. We have proposed the phase diagram of CLRO. Main conclusions are as follows:

- Non-metallic ground state with canted antiferromagnetic order is realized for $0.00 \leq x < 0.15$. The ground state is in a broad sense Mott insulator, but more precisely consistent with the Anderson localization state with Coulomb interaction.
- Filling control of Ca_2RuO_4 drastically changes the metallic ground state ($x > 0.10$) adjacent to CAF-NM ground state compared with purely bandwidth controlled CSRO. We did not find any sign of superconductivity at least down to 50 mK. FM fluctuation is strong in this region.

Acknowledgements

We would like to thank T. Ishiguro for his support in many aspects. We acknowledge useful discussion with S. Nakatsuji and his technical support. We appreciate T. Mizokawa for fruitful discussion. We are grateful to K. Kosuge, K. Yoshimura and M. Kato for permitting the authors to use EDX apparatus and for their kind help. One of the authors (H. F.) is supported by JSPS Research Fellowships for Young Scientists.

-
- [1] Y. Maeno, H. Hashimoto, K. Yoshida, S. Nishizaki, T. Fujita, J. G. Bednortz and F. Lichtenberg: *Nature* **372** (1994) 532.
 [2] K. Ishida, H. Mukuda, Y. Kitaoka, K. Asayama, Z. Q. Mao, Y. Mori and Y. Maeno: *Nature* **396** (1998) 658.
 [3] A. P. Mackenzie, R. K. W. Haselwimmer, A. W. Tyler, G. G. Lonzarich, Y. Mori, S. Nishizaki and Y. Maeno: *Phys. Rev. Lett.* **80** (1998) 161.
 [4] Z. Q. Mao, Y. Maeno, S. Nishizaki, T. Akima and T. Ishiguro: *Phys. Rev. Lett.* **84** (2000) 991.

- [5] S. Nishizaki, Y. Maeno and Z. Q. Mao: *J. Phys. Soc. Jpn.* **69** (2000) 572.
 [6] Y. Maeno, K. Yoshida, H. Hashimoto, S. Nishizaki, S. Ikeda, M. Nohara, T. Fujita, A. P. Mackenzie, N. E. Hussey, J. G. Bednortz and F. Lichtenberg: *J. Phys. Soc. Jpn.* **66** (1997) 1405.
 [7] H. Mukuda, K. Ishida, Y. Kitaoka, K. Asayama, Z. Q. Mao, Y. Mori and Y. Maeno: *J. Phys. Soc. Jpn.* **67** (1998) 3945.
 [8] S. Nakatsuji, S. Ikeda and Y. Maeno: *J. Phys. Soc. Jpn.* **66** (1997) 1868.
 [9] G. Cao, S. McCall, M. Shepard, J. E. Crow and R. P. Guertin: *Phys. Rev. B* **56** (1997) R2916.
 [10] M. Braden, G. André, S. Nakatsuji and Y. Maeno: *Phys. Rev. B* **58** (1998) 847.
 [11] C. S. Alexander, G. Cao, V. Dobrosavljevic, S. McCall, E. Lochner and R. P. Guertin: *Phys. Rev. B* **60** (1999) R8422.
 [12] H. Fukazawa, S. Nakatsuji and Y. Maeno: *Physica B* **281 & 282** (2000) 613.
 [13] S. Nakatsuji and Y. Maeno: *Phys. Rev. Lett.* **84** (2000) 2666.
 [14] S. Nakatsuji and Y. Maeno: to be published in *Phys. Rev. B* **62** (2000) Sep. 1 issue.
 [15] O. Friedt, M. Braden, G. André, P. Adelman, S. Nakatsuji and Y. Maeno: cond-mat/0007218.
 [16] The structural symmetry associated with longer lattice parameter c along the long axis is denoted as L-Pbca: in contrast, the one with shorter c parameter is denoted as S-Pbca.
 [17] V. I. Anisimov, I. A. Nekrasov, D. E. Kondakov, T. M. Rice and M. Sigrist: preprint.
 [18] G. Cao, S. McCall, V. Dobrosavljevic, C. S. Alexander, J. E. Crow and R. P. Guertin: *Phys. Rev. B* **61** (2000) R5053.
 [19] The difference is especially significant in the bilayered perovskite $\text{Sr}_3\text{Ru}_2\text{O}_7$. For references, we cite two representative papers: for a FZ method, S. Ikeda, Y. Maeno, S. Nakatsuji, M. Kosaka and Y. Uwatoko: to be published in *Phys. Rev. B* **62** (2000) Sep. 1 issue. (cond-mat/0002147); for a flux method, G. Cao, S. McCall and J. E. Crow: *Phys. Rev. B* **55** (1997) R672.
 [20] NEC Machinery, model SC-K15HD.
 [21] Quantum Design, model MPMS55. We used an additional insert equipped with an oven for the measurement between 300 and 700 K.
 [22] A. P. Mackenzie, S. Ikeda, Y. Maeno, T. Fujita, S. R. Julian and G. G. Lonzarich: *J. Phys. Soc. Jpn.* **67** (1998) 385.
 [23] T. Moriya and A. Kawabata: *J. Phys. Soc. Jpn.* **35** (1973) 669.
 [24] I. I. Mazin and D. J. Singh: *Phys. Rev. Lett.* **82** (1999) 4324.
 [25] I. I. Mazin and D. J. Singh: private communication.
 [26] T. Mizokawa, L. H. Tjeng, G. A. Sawatzky, G. Ghiringhelli, O. Tjernberg, N. B. Brookes, H. Fukazawa, S. Nakatsuji and Y. Maeno: preprint.
 [27] K. Yosida: *Theory of Magnetism* (Springer-Verlag, Berlin, 1996) pp. 38.
 [28] $\overline{\chi_{ab}}$ becomes smaller than χ_c again below about 150 K. However, it is owing to the reduction of $\chi_{[010]}$ associated with the evolution of short-range AF correlation above T_N .¹²⁾
 [29] N. F. Mott: *Metal-Insulator Transitions*, 2nd ed. (Taylor & Francis, London, 1990) Chap. 1.
 [30] A. L. Efros and B. I. Shklovskii: *J. Phys. C* **8** (1975) L49.
 [31] A. V. Puchkov, M. C. Schabel, D. N. Basov, T. Startseva, G. Cao, T. Timusk and Z. -X. Shen: *Phys. Rev. Lett.* **81** (1998) 2747.
 [32] T. Oguchi: *Phys. Rev. B* **51** (1995) 1385.
 [33] T. Nomura and K. Yamada: *J. Phys. Soc. Jpn.* **69** (2000) 1856.